Atomic Scale Observation of the Structural Dynamics of Supported Gold Nanocatalysts under 1,3-Butadiene by in situ Environmental Transmission Electron Microscopy

Abdallah Nassereddine, Laurent Delannoy, Christian Ricolleau, Catherine Louis, Alloyeau D., Guillaume Wang, Qing Wang, Hazar Guesmi, Jaysen Nelayah

ChemCatChem

The European Society Journal for Catalysis

Chemistry Europe

European Chemical Societies Publishing

Supported by GECATS GERMAN CATALYSIS SOCIETY

Accepted Article

Title: Atomic Scale Observation of the Structural Dynamics of Supported Gold Nanocatalysts under 1,3-Butadiene by in situ Environmental Transmission Electron Microscopy

Authors: Abdallah Nassereddine, Laurent Delannoy, Christian Ricolleau, Catherine Louis, Damien Alloyeau, Guillaume Wang, Qing Wang, Hazar Guesmi, and Jaysen Nelayah

To be cited as: *ChemCatChem* **2023**, e202300434

Link to VoR: https://doi.org/10.1002/cctc.202300434

WILEY VCH

10.1002/cctc.202300434

Atomic Scale Observation of the Structural Dynamics of Supported Gold Nanocatalysts under 1,3-Butadiene by *in situ* Environmental Transmission Electron Microscopy

Abdallah Nassereddine,* [a,b] Laurent Delannoy,[c] Christian Ricolleau,[a] Catherine Louis,[c] Damien Alloyeau,[a] Guillaume Wang,[a] Qing Wang,[d] Hazar Guesmi,[d] and Jaysen Nelayah*[a]

[a] Dr. Abdallah Nassereddine, Prof. Christian Ricolleau, Dr. Damien Alloyeau, Dr. Guillaume Wang, Dr. Jaysen Nelayah
Université Paris Cité, CNRS, Laboratoire Matériaux et Phénomènes Quantiques
10 rue Alice Domon et Léonie Duquet, 75013 Paris, France
E-mail: abdallah.nassereddine@esrf.fr and jaysen.nelayah@u-paris.fr

[b] Dr. Abdallah Nassereddine
Institut Néel, Université Grenoble Alpes, CNRS
25 Avenue des Martyrs, 38042 Grenoble, France

[c] Dr. Laurent Delannoy, Dr. Catherine Louis
Laboratoire de Réactivité de Surface, Sorbonne Université, CNRS
4 place Jussieu, 75005 Paris, France

[d] Dr. Hazar Guesmi, Dr. Qing Wang
ICGM, Univ. Montpellier, CNRS, ENSCM
919 Rte de Mende, 34293 Montpellier Cedex 5, France

Supporting information for this article is given via a link at the end of the document

Abstract

Supported gold catalysts have been reported to exhibit exceptional selectivity towards the desirable product, an alkene, in chemoselective hydrogenation of highly unsaturated alkynes and alkadienes. However, insights on the interactions between the gold nanoparticles and the 1,3-butadiene adsorbates are lacking. In this work, using atomic scale *in situ* ETEM with the support of DFT-based calculations, we investigate the reactivity of TiO_2 supported gold nanoparticles below 7 nm towards 1,3-butadiene by monitoring their structure and dynamics under 10^5 Pa of 0.46% C_4H_6/He during cooling at 300°C and 200 °C. For size larger than 5 nm, the initial truncated octahedron morphology of gold nanoparticles is found to evolve towards a rounded morphology, with the growth of more open (110) surfaces and higher index facets at the expense of the initially present (100) and (111) facets, reflecting the adsorption of butadiene on low coordination sites at 300 °C. The morphology changes are shown to be accompanied by nucleation and glide of dislocations. At 200 °C, butadiene adsorption is shown to be predominant on (111) facets, with the nanoparticles reverting to a faceted morphology. For smaller particle size, a rounded morphology is maintained under 1,3-butadiene.

Introduction

While bulk gold is chemically inert and is generally regarded as a poor catalyst, gold dispersed on supports as atoms, clusters and nanoparticles (Au NPs) have been shown to be highly effective in various chemical reactions for environmental and industrial interests, both as oxidation and hydrogenation catalysts.[1-5] Among other studies, several have shown that highly dispersed Au NPs on metal oxide exhibit excellent selectivity for hydrogenation of multiple functional groups, such as the chemoselective hydrogenation of poly-unsaturated hydrocarbons like alkynes and alkadienes (C_2-C_6) to alkenes.[6,7] This type of reaction is a critical process in the chemical industry. For example, in the case of C_4-cut hydrocarbon streams, selective hydrogenation of 1,3-butadiene impurities produces high purity butene streams known as an important raw material for polymer production.[6,8]

Historically, the first study of 1,3-butadiene hydrogenation over gold catalysts was conducted by Bond *et al.* in the early 1970s.[9-11] They reported that when the reaction occurred between 130 and 260 °C, Al_2O_3- and SiO_2-supported Au catalysts could selectively hydrogenate the 1,3-butadiene into butenes. In 2002, Okumura *et al.* showed that Au NPs supported on TiO_2, Al_2O_3 and SiO_2 were also able to partially hydrogenate the 1,3-butadiene with 100 % selectivity of butenes at around 180 °C **[12]**. Few years later, Hugon *et al.* studied the selective hydrogenation of 1,3-butadiene in conditions closer to those of purification (i.e., in excess of alkenes).[13,14] They confirmed that various supported (Al_2O_3,

CeO_2, ZrO_2 and TiO_2) Au NPs in the size range from 2 to 5 nm were able to convert all the butadiene to butenes at 170 °C, with only very limited hydrogenation of alkenes to alkanes.

The hydrogenation of 1,3-butadiene gas molecule over Au heterogeneous catalysts has been mainly described on the basis of the Horiuti-Polanyi mechanism,[15-17] although some recent studies have proposed that a non- Horiuti-Polanyi mechanism could also be considered [18]. In the Horiuti-Polanyi mechanism, H_2 molecules are first dissociated into atomic H on Au NPs followed by the addition of the latter to the adsorbed 1,3-butadiene molecules. The dissociative adsorption of H_2 on the Au NPs surface is generally considered as the rate determining step in the hydrogenation process over gold catalysts.[14,19-21] The catalytic activity of Au NPs in selective hydrogenation reactions thus depends on their catalyst capacity to adsorb and dissociate H_2. On the other hand, the high selectivity towards butenes is driven by the adsorption of 1,3-butadiene molecules on the Au NPs as well that react with adsorbed H.[22]

Numerous experimental and theoretical studies have been carried out on the adsorption and dissociation of H_2 molecules by supported Au.[23] It has been shown experimentally that the reactivity of gold towards hydrogen increases with decreasing particle size, and that the highest reactivity is observed for particles smaller than about 4 nm.[24] Several studies have hinted that with a decrease in the size of Au NPs, an increase in the proportion of surface atoms is observed, particularly low-coordination atoms on the corners and edges of the NPs, promoting hydrogen dissociation on the surface of the NPs, without modifying the structure or morphologies of particles.[21,25-28] The concept of fluxionality (or structural flexibility) has also been introduced to explain the particular reactivity of small Au clusters.[29-31]

Surprisingly, the reactivity of Au nanoparticles towards 1,3-butadiene adsorption has been scarcely studied in the literature and to our knowledge the few experimental and theoretical works published in the literature are mainly focusing on the adsorption mechanisms. Ten years ago, joint experimental and theoretical investigations were performed by X.F Yang and coworkers[22] to study the selectivity of gold catalysts in hydrogenation of 1,3-butadiène toward cis-2-Butene. Their DFT calculations performed on Au(100) surface and Au_{19} cluster models show that the cis-1,3-butadiene strongly adsorbs on under coordinated sites of gold compared to the trans-1,3-butadiene which explains the unusual measured selectivity of gold nanocatalysts toward forming cis-2-butene. In addition, based on orbital interaction analyses these authors show that Au-6s-based molecular orbitals prefer the adsorption of cis-1,3-butadiene to the trans isomer due to spatial match. In a recent work, using extensive density functional calculations and microkinetic modeling, Yang *et al.*[18] have reported the reaction pathway of the hydrogenation mechanism of 1,3-butadiene by taking Au(211) flat surface as a termination to represent the active sites with low coordination gold atoms. However, the lack of information about the realistic surface structure and the nature of the active gold sites operating under reactive media render questionable all these interpretations.

For this concern, D.J. Martin, *et al.* performed GISAXS/GIWAXS study under *operando* conditions to study the surface state of SiO_2-supported Au nanoparticles during butadiene hydrogenation. These authors revealed that gold nanoparticles undergo reversible size, shape and phase changes.[32] During butadiene hydrogenation, it was observed an increase in particle height from 4.8 to 9.3 nm leading to a change in particle morphology with a taller aspect ratio (the NP radius only increases marginally by ca. 0.45 nm). However, when returning under inert atmosphere (He at 200 °C), Au NPs regain their initial size and morphology. Apart from this study, no direct *in-situ* observation of the gold catalysts was observed under pure butadiene, allowing identification of the effect of the butadiene molecule adsorption on the structure and morphology of Au NPs. Thus, the reactivity of butadiene molecules with Au NPs is yet to be explored experimentally.

The evaluation of the reactivity of Au NPs under reactive gases requires access to experimental approaches allowing the monitoring of their structural evolution under appropriate pressure and temperature conditions. In this regard, *in situ* environmental transmission electron microscopy (ETEM) provides the unique capability to characterize the gas-nanoparticles dynamic interactions.[33,34] In recent years, tremendous benefits have been gained from using *in situ* ETEM technique with the advancement of TEM aberration correction and windowed gas cells, allowing the observation, at atomic-scale and in real time, of the structural dynamics of NPs at high pressure and high temperature.[35,36] *In situ* ETEM has emerged as a highly effective technique for tracking the dynamic evolution of various types of nanomaterials, including single atoms, clusters, nanocrystals, and low dimensional materials. This technique offers real-space imaging capabilities with sub-angstrom spatial resolution, microelectron volt energy resolution, and millisecond time scales, making it a highly

advanced tool for studying the atomic-scale structural dynamics of nanomaterials.[37] In the field of heterogeneous catalysis, numerous studies have demonstrated the effectiveness of this technique in investigating the structural dynamics of catalysts [37,38] and their interaction with the support [39,40] under reaction conditions. Furthermore, ETEM technique has provided ample evidence that a strong-metal strong interaction (SMSI) is present in the classical TiO_2 system, as demonstrated in several studies. [41,42,43]

In our recent work, we benefited from the ETEM to study the reactivity of Au NPs under H_2 at atomic-scale.[44] By combining *in situ* ETEM observations with *ab initio* molecular dynamics simulations, we evidenced a size-dependent reactivity of Au NPs under H_2, and we showed the existence of a critical size (4 nm) below which the dissociative adsorption of H_2 is activated on the Au NPs. We also showed, for the first time, that the gain in reactivity of Au NPs smaller than 4 nm is accompanied not only by a modification of their surface, but also by a transformation of their core structure from faced-centre cubic (fcc) to non-fcc types under working conditions. In order to gain further fundamental insights into butadiene hydrogenation reaction (where gold both interact with hydrogen and butadiene) it is mandatory to perform a parallel study of the reactivity of Au nanoparticles under butadiene pressure, which is the subject of this work. Herein, *in situ* ETEM was used, for the first time, to monitor structural dynamics of TiO_2 supported active Au nanoparticles with size ranging from 1 to 7 nm under atmospheric pressure of 0.46% C_4H_6/He mixture. We observed a continuous evolution of the morphology of Au NPs at different temperatures, accompanied by subsurface dislocations, nucleation and stacking fault stabilization in the core of the NPs. These observations, confirmed by Density Functional Theory (DFT)-based MultiScale Reconstruction (MSR) model, show temperature dependence of the adsorption of the 1,3-butadiene. In addition, likewise hydrogen, 1,3-butadiene is found to induce size dependent morphology changes but the faced-centre cubic structure remains stable whatever the applied temperature.

Results and discussions

Temperature dependent structure evolution of Au NPs > 5 nm under 1,3-butadiene

To gain experimental insights in the reactivity of 1,3-butadiene with nanoparticles of gold, we studied by *in situ* gas TEM the structure of Au NPs supported on anatase TiO_2 and their dynamics upon exposure to 1,3-butadiene. Au NPs studied in this paper were obtained from the same batch of the as-prepared Au/TiO_2 particles investigated in our recent work on the reactivity of Au NPs in H_2 environment.[44] The gold nanoparticles have a size distribution ranging from 1 to 7 nm, with an average size of 3.5 nm. Additionally, the as-prepared Au/TiO_2 nanoparticles were observed *ex situ* using high-resolution high-angle annular dark-field scanning transmission electron microscopy, which revealed that the Au NPs have a fcc structure. **Figure 1.A** shows a temperature series of atomic resolution high-angle annular dark-field scanning ETEM (HAADF-STEM) of a 5 nm Au NP at 300 °C and 200 °C under 10^5 Pa of 0.46% C_4H_6 balanced by He. The NP is here viewed in projection parallel to the metal-oxide interface. The series of bright field (BF-STEM) images acquired in parallel and the corresponding fast Fourier transform (FFT) patterns of the HAADF-STEM images are shown in Figure 1.B and C respectively. The experiment workflow followed in the present work to study the reactivity of Au NPs with 1,3-butadiene was developed and used in our previous works to reveal the reactivity toward O_2 and H_2 molecules with the same Au/TiO_2 system.[28,37] Thus, before exposure to 1,3-butadiene, reference STEM HAADF and BF images of the Au NP under residual argon (~ 50 Pa) were acquired at a temperature of 300 °C. Under Ar, the Au NP displays a fcc symmetry structure viewed close to the [101] zone axis (**Figure 1.A-C a**). The 2D projection of the NP is consistent with a truncated octahedron (TOh) morphology exposing wide (100) and (111) facets (**Figure 1.A,B a**). In contrast to Au TOh NPs in the same size range which showed no significant morphology change, so little tendency to adsorb H_2 molecules,[37] the 5 nm Au NP shows major changes in morphology upon exposure to 1,3-butadiene between 300 and 200 °C, reflecting the adsorption of butadiene molecules on the particle surface.

10.1002/cctc.202300434

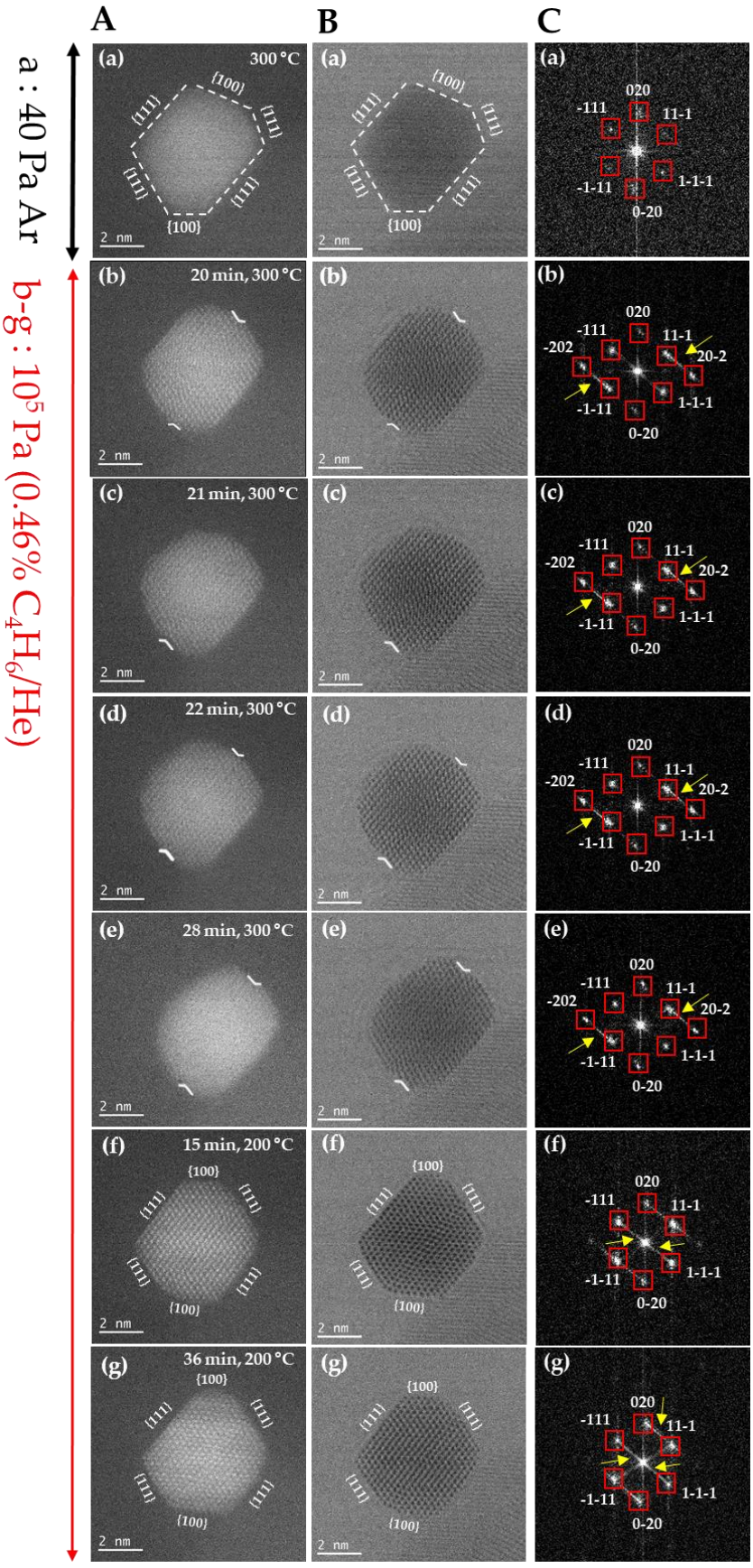

Figure 1. Atomic scale visualization of the structural evolution of a ~5 nm Au NP supported on anatase TiO_2 in 0.46% C_4H_6/He gas mixture at atmospheric pressure. **(A)** HAADF-STEM and **(B)** BF-STEM images of the NP acquired *in situ* at **(a)** 300 °C under 40 Pa Ar, **(b-e)** 300 °C and **(f-g)** 200 °C under 10^5 Pa of 0.46% C_4H_6/He showing a continuous evolution of the morphology of the NP. **(C)** FFT of the HAADF-STEM images showing

a stable fcc crystalline structure of the NP between 300 and 200 °C. The NP is viewed close to the [101] direction of the fcc structure. The broken white lines in **(a)** highlight the projected truncated octahedral equilibrium shapes of the NP in Ar at 300 °C. The reentrant facets imaged at 300 °C are indicated by chevrons in (**A,B b-e)**.

As 1,3-butadiene is introduced at 300 °C, the particle morphology evolves continuously towards a hemisphere with small reentrants edges visible after 28 minutes of exposure (**Figure 1.A,B a-e).** This morphology changes result from the growth of (110) and high Miller index crystal facets (h ≥ 2, k ≥ 1, l ≥ 1), with high density of low-coordination atomic sites [45] at the expense of the initially present (100) and (111) facets. In contrast, decreasing the temperature to 200 °C under 1,3-butadiene leads to further faceting of the surface of Au NP with the reappearance and expansion of the (111) facets after 15 minutes at this temperature (**Figure 1.A,B f**). However, the morphology stabilized at this temperature is different from a TOh and remains stable up to 36 minutes of exposure to 1,3-butadiene. The fraction of (111) facets is found to be higher than under Ar (comparison of **Figures 1.A,B a** and **g**).

The morphology of a second Au NP of 7 nm in diameter was followed under the same temperature and pressure conditions. We observe that this NP undergoes similar morphology dynamics, displaying a rounded morphology at 300 °C under butadiene that evolves towards a faceted morphology as the NP is cooled down to 200 °C (**Figure S1**). *In situ* tracking of the morphology of the two Au NPs tend to suggest that the (110) surface sites of these gold nanoparticles in the range from 5 to 7 nm are active towards butadiene adsorption at 300 °C but that at 200 °C, butadiene adsorption becomes again predominant on (111) facets, leading back to faceted Au NPs. In the size and temperature range studied, no such faceting-roughening was observed for Au NPs under atmospheric pressure H_2.[28,44] Furthermore, the monitoring of the structural evolution of a smaller Au NP (2.2 nm) exhibits the same behavior in terms of crystalline structure. As shown in the **Figure S2**, the monitoring of the distances between the (111) planes on the HAADF-STEM images shows a lattice parameter similar to bulk gold (within the measurement uncertainties), signature of a strong structural stability of the NP under Ar and 1,3-butadiene at 200 °C. In our previous work, Au NPs in the same size range and exposed to H_2 at atmospheric pressure were found to undergo strong structural evolutions in the same temperature range, while larger Au NPs were stable and maintained their fcc structure.[44] The *in situ* ETEM observations made here under butadiene show the absence of such size effects on crystalline structure in the presence of butadiene.

In order to understand this puzzling behavior and to confirm our interpretation of these observed changes, we applied the DFT-based MultiScale Reconstruction (MSR) model in attempt to qualitatively predict the shape evolution of gold NPs in presence of butadiene. This model, that has been shown to be effective for many systems,[28,46,47] consists of using Wulff construction theorem to predict the thermodynamic equilibrium shapes of the Au NPs based on calculated DFT interface tensions evolving as a function of temperature and pressure (see theoretical details in Experimental section and SI). In **Figure 2.a**, the evolution of the calculated interface tension of different computed (111), (100) and (110) facets of gold NP for temperature between 27°C and 900°C and in presence of butadiene at 1 bar pressure is reported. All DFT energetic values used for the calculations of interface tension are depicted in Table 1 in the SI. In **Figure 2b**, the shape evolution of the constructed gold NP of size around 5 nm is represented by the variation of average coordination number ($\overline{CN}$) which is obtained by calculating the total coordination number (CN) of each surface atom and then the average value (see theoretical details).

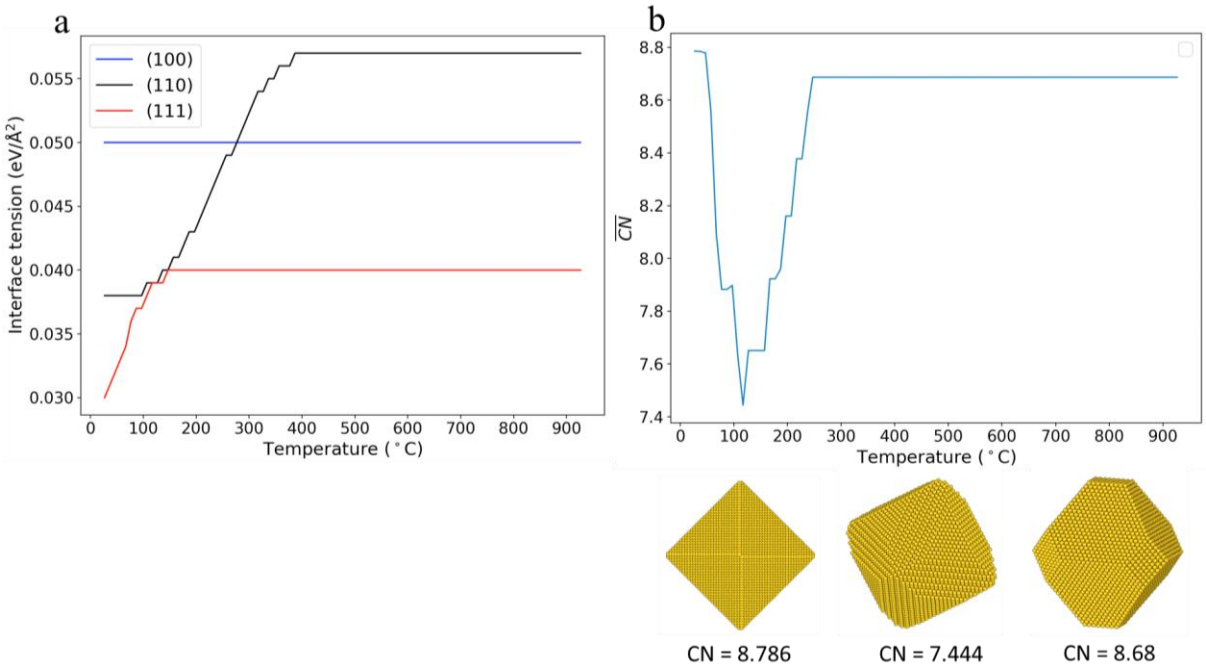

Figure 2. Shape evolution under butadiene of Au NP of size about 5nm predicted by DFT based MSR model. Calculated evolution of **(a)** interface tension of the (111), (100) and (110) facets and **(b)** average coordination numbers of surface atoms as a function of temperature.

The obtained results confirm the important morphology changes that the Au NP undergoes under butadiene as a function of temperature. For high temperature (which is equivalent to the observations under near-vacuum conditions under residual argon), the calculated interface tensions (**Figure 2a**) follow the expected stability order of (111) > (100) > (110) leading to the stabilization of the Au NP in truncated octahedron (TOh) morphology exposing wide (100) and (111) facets, which is in full agreement with experimental observations. When the temperature decreases, the adsorbed butadiene, with calculated adsorption energy in the order of E_{ads110} (|-0.9| eV) > E_{ads111} (|-0.45| eV) > E_{ads100} (|-0.2| eV) (see Table SI in supplementary Information), leads to the growth of the (110) facet at the expense of the other two facets. Interestingly, the stronger stability of the (110) facet is found to occur within a narrow window of temperature (between 75and 175 °C) where the Au NP would be rounded with an average coordination number of surface atoms of 7.44. This finding is in good agreement with the ETEM results, i.e. rounded Au NPs shape appearing at 300°C and disappearing for temperature lower than 200°C, and confirms the strong preference of butadiene to adsorb over under coordinated Au sites. Additionally, further decrease of the temperature leads to the disappearance of the (110) facets and reappearance and expansion of the (111) facets in full agreement with the experimental observations. It is to be noted that the predicted theoretical temperatures are shifted by about 125°C with respect to the experimental ones which may be due to underestimated values of calculated surface energies which is a known artifact of DFT methods.[48] Apart from this, the provided qualitative prediction of the thermodynamic equilibrium shapes of Au NP highly supports the experimental observed dynamics and confirms the temperature dependence of the reactivity of gold NP of size larger than 5 nm toward butadiene adsorption.

Movement of dislocations in the gold particle core: the starting point of morphology transition?

While the particle morphology and the crystalline structure of the particle-oxide interface evolve continuously upon butadiene exposure, indexing of the FFT of the HAADF-STEM images shows that the 5 nm Au NP retains a fcc structure and its orientation with respect to the TiO_2 support during cooling from 300 to 200 °C under 1,3-butadiene (**Figure 1.C b-g**). Moreover, close examination of the FFT shows the presence of diffuse streaks between the spots of the FFT patterns at 300 and 200 °C (highlighted by yellow arrows on **Figure 1.C b-g**). As discussed in literature,[49] M.A. Asadabad *et al.* showed that such streaks are an indication of the presence of linear and planar lattice defects in the core of the NP (dislocations, twin boundaries, stacking faults). Atomic scale analysis of the structure of Au NP from the BF-STEM images

in **Figure 3** confirms that the changes in particle morphology under butadiene result from the nucleation and movement of dislocations in the particle core.

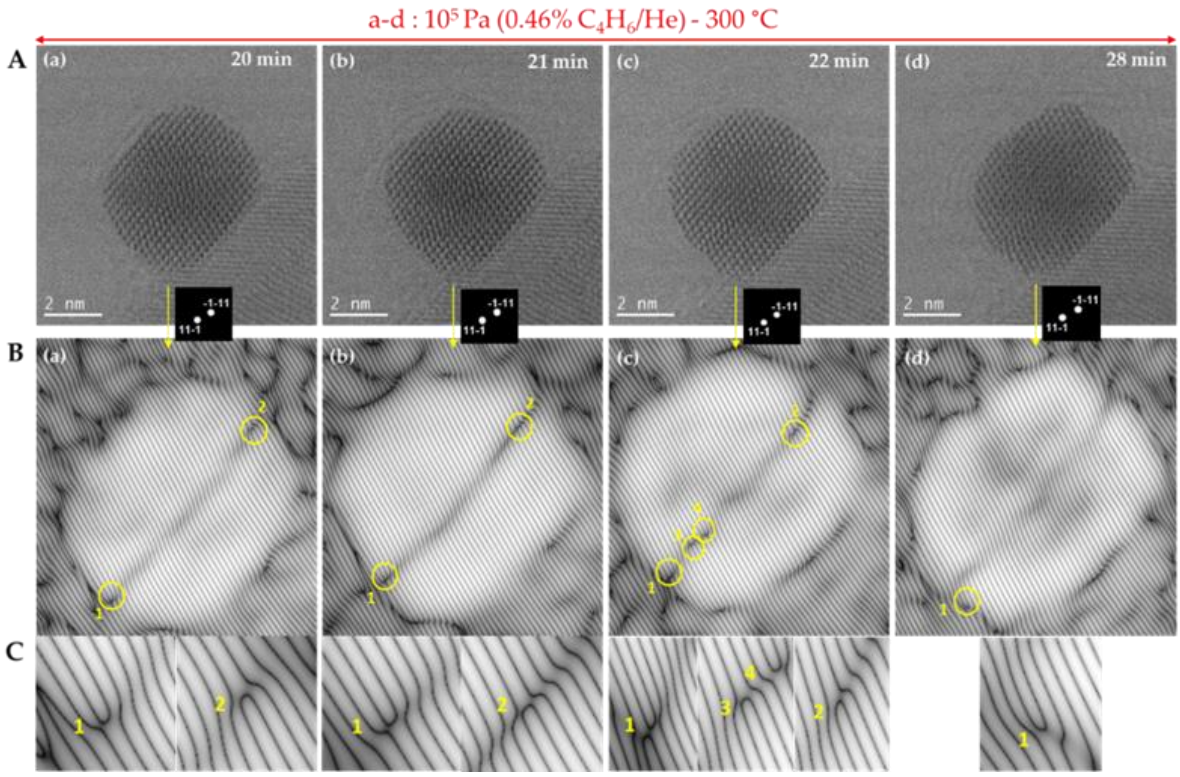

Figure 3. Morphology change driven by the nucleation and gliding of edge dislocations **(A)** *In situ* BF-STEM images of Au NP under 10^5 Pa of 0.46% C_4H_6/He at 300 °C. **(B)** Corresponding Bragg filtered images obtained by Fourier mask filtering the (-1-11) and (11-1) spots in the FFT. The position of the edge dislocations are indicated by yellow circles. **(C)** Zooms-in of the encircled areas in **(B)** showing the structure of the dislocations identified.

To better visualize these dislocations, we applied a Bragg filter[50] on the FFT pattern of the time series of BF-STEM images of the NP under 1,3-butadiene at 300 °C (**Figure 3.A**). The resulting Bragg-filtered images are shown in **Figure 3.B.a**. After 20 minutes under butadiene at 300 °C, two edge dislocations with dislocation lines perpendicular to the image plane are observed near the particle surface at the re-entrant corners highlighted in **Figure 1A.b**. The dislocations are numbered 1 and 2 with the positions of the dislocation lines circled in yellow. As the NP is maintained under these conditions for further two minutes, we observe the gradual gliding of dislocation 2 and the nucleation of two additional edge dislocations denoted as 3 and 4 close to dislocation 1 (**Figure 3.B.a-c**). Zooms-in of the Bragg-filtered images around the dislocations in Figure 3.C show the positions of the four corresponding (111) half-planes. After 28 minutes at 300 °C, only one edge dislocation prevails (**Figure 3.B.d**) while after 15 minutes at 200 °C, no dislocation is observed (**Figure 1.f,g**).

The drastic morphological changes undergone by the 5 nm Au NP under 1,3-butadiene at 300 °C accompanied by the nucleation and gliding of dislocations provides a strong evidence that the NP undergoes plastic deformation upon adsorption of the butadiene molecules. Such deformation implies strong interactions between butadiene and the Au nanoparticles which, at this temperature, have many low coordination sites on the surface (resulting from the roughening of the surface). These observations are consistent with the review work by Bond[4] in which it was suggested, based on the kinetics calculation of the apparent reaction orders with respect to H_2 and alkenes/alkadienes during hydrogenation reactions of unsaturated hydrocarbons, that alkenes and alkadienes are quite strongly adsorbed on the active sites but without inhibiting H_2 adsorption. An order of reaction for butadiene close to zero was indeed reported for supported gold catalysts and reflects this strong, but not inhibiting, adsorption of the alkadiene molecule.[14,51]

10.1002/cctc.202300434

The BF-STEM images of the 5 nm Au NP acquired after 15 and 36 minutes under 1,3-butadiene at 200 °C clearly show that the evolution of the NP morphology to a faceted morphology at this temperature is accompanied by a rearrangement of the close-packed (111) planes at the core of the particle, leading to the stabilization of two stacking faults (**Figure 4**). The positions of the stacking faults are represented by white broken lines on **Figure 4**.

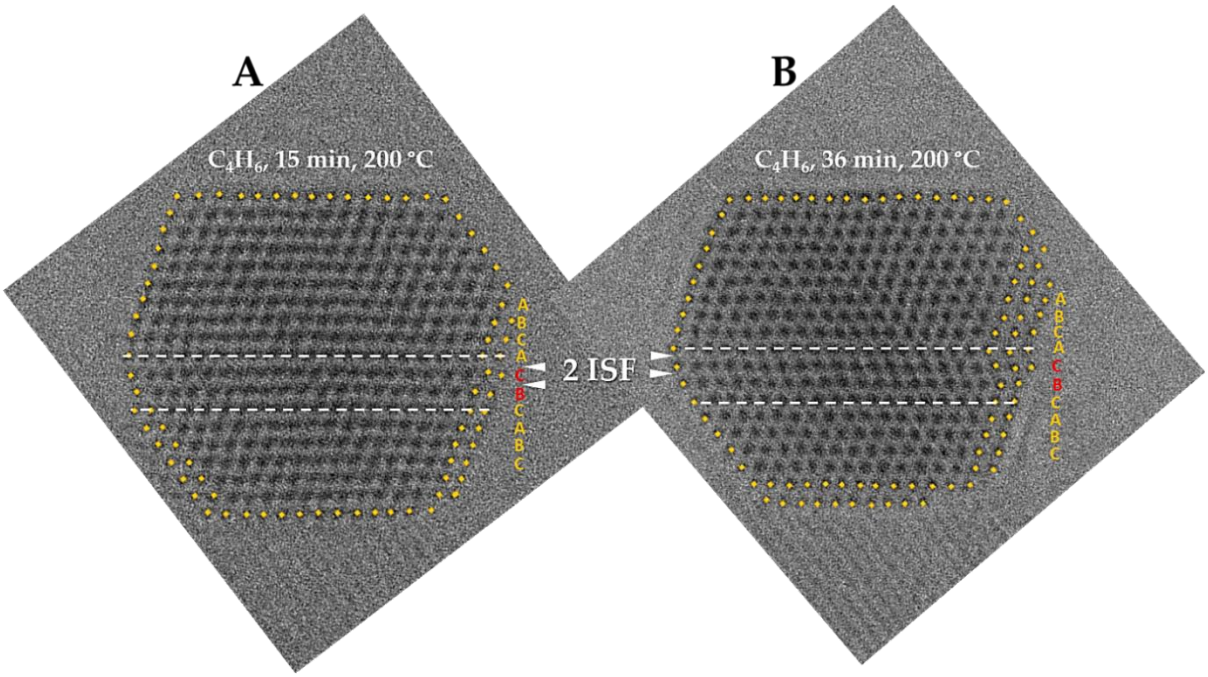

Figure 4. *In situ* atomic resolution BF-STEM images of Au NP showing the indexed stacking sequence of the closed-packed planes along the [111] crystallographic direction after **(A)** 15 minutes and **(B)** 36 minutes of exposure under 10^5 Pa of 0.46% C_4H_6/He at 200 °C. The plane labels are represented by the ABCA… letters. The region between the two broken white lines in both images corresponds to the region in which the intrinsic stacking faults (ISF) are formed.

The analysis of the stacking sequence of the compact planes in the Au[111] direction shows that these stacking faults are of intrinsic type, corresponding to two missing (111) planes in the core of the NP (**Figure 4.A**). Moreover, the crystalline structure of the particle no longer evolves when it is maintained for a further 21 minutes under 1,3-butadiene at 200 °C (**Figure 4.B**). This is a strong indication that the creation of stacking faults is energetically favoured under the prevailing temperature and pressure conditions. It has been shown that stacking faults can strongly and favorably affect catalytic activity of nanomaterials.[52-54] Notably, it was found that stacking faults by jointly introducing low coordination surface sites and high tensile strain could improve adsorption of reactants on a catalyst.[53]

Atomic scale analysis of particle-oxide interface

The investigation of the gold lattice structure at the particle-oxide interface also shows interesting behavior with changes in the wetting properties of the 5 nm gold NP at the contact surface with the TiO_2 support. **Figure 5** shows zoomed-in BF images of the particle-TiO_2 interface as the Au NP morphology evolves under 1,3-butadiene.

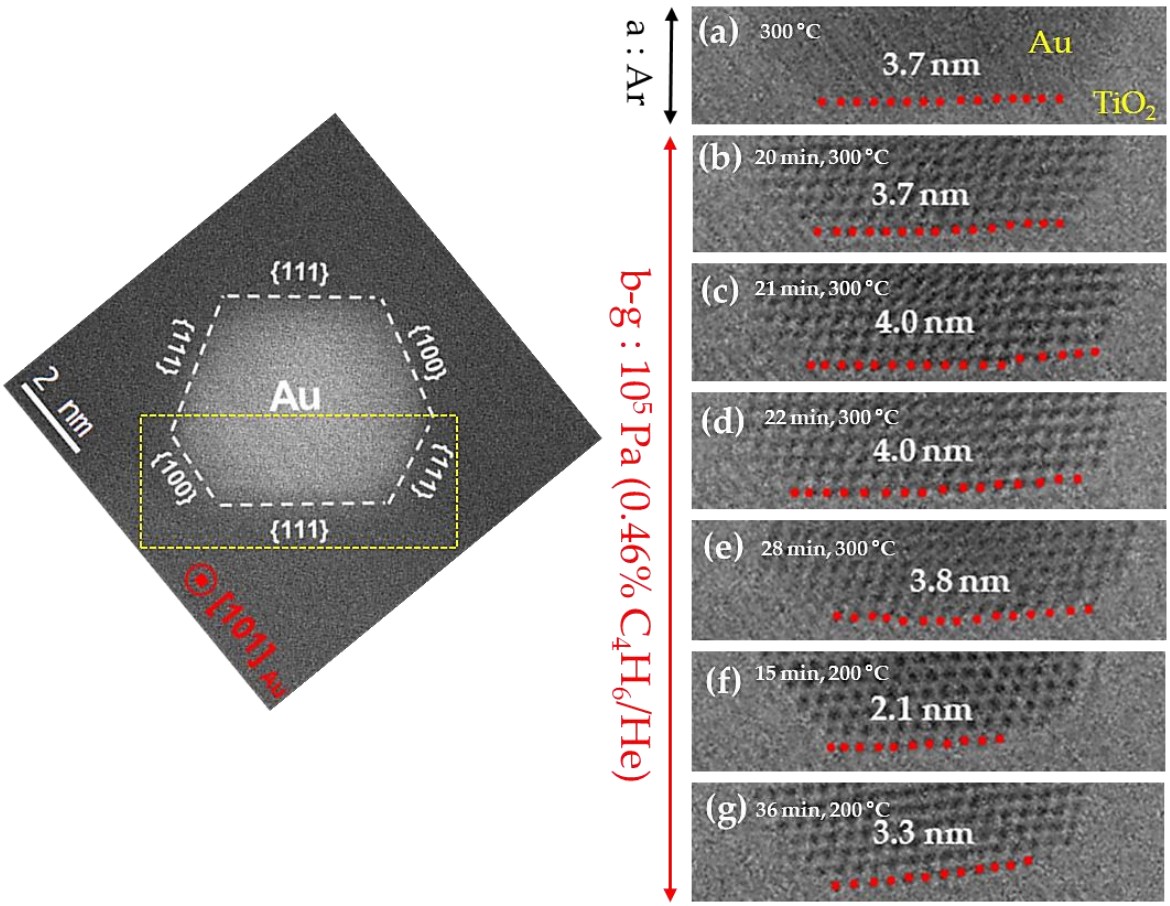

Figure 5. Zoom-in images of the particle-oxide interface of the nanoparticle in Figure 1 showing the continuous evolution of the wetting properties under **(a)** Ar and **(b-g)** C_4H_6. The atomic layer of Au in contact with the support is highlighted by red dots. Particle orientation and mean position on the support was found to be relatively stable.

The follow-up of the gold lattice plane in contact with oxide support show a continuous variation of the extension of the Au-TiO_2 interface, which indicates a continuous wetting and dewetting of Au NP during heating at 300 °C and 200 °C respectively under 1,3-butadiene. No diffusive motion of the particle on the support is observed. These wetting-dewetting phenomena may reflect the adsorption of butadiene on low coordination sites of gold located at this particle-support interface. It should be however noted that in the present case, the exact structure of the interface is not known since the signal to noise ratio and STEM contrast in the oxide region is not sufficient enough to clearly resolve the atomic structure of the anatase support. The image blurring in the oxide region is likely due to important electron scattering through the entire thickness of the TiO_2 support (~30 nm).

Conclusion

A combined experimental and theoretical approaches were used to understand the reactivity of TiO_2 supported gold nanoparticles towards 1,3-butadiene gas by monitoring their structure and dynamics at high temperature/pressure catalytic conditions. Atomic scale *in situ* ETEM observations at 300 and 200 °C show the evolution of particle structure as a function of the applied temperature, which indicates the adsorption of butadiene on Au NPs. This study shows that the adsorption of 1,3-butadiene on Au NPs strongly depends on temperature. For NPs size between 5-7 nm, the initial truncated octahedron morphology is found to evolve towards a rounded morphology, with the growth of more open (110) surfaces and higher index facets at the expense of the initially present (100) and (111) facets, attributed to the high affinity of butadiene to low coordinated at 300 °C. The decrease in temperature at 200 °C induces nucleation and glide of dislocations followed by the development of stacking faults showing the first steps of morphology changes under catalytic conditions. In this case, the stronger stability of the (110) facet is found to occur within a narrow window of temperature

(between 75 and 175°C). Throughout their morphological transformation, the NPs maintain a fcc structure. The preservation of gold fcc structure is evidenced at particle size as small as 2 nm. This research describes, the first experimental observations of the effect of 1,3-butadiene adsorption on the active sites of gold catalysts, and open up an alternative avenue for the understanding of the mechanism of the industrially relevant selective hydrogenation of 1,3-butadiene molecule with gold catalysts.

Experimental Section

Sample preparation

6 wt% Au/TiO_2 catalyst was prepared by the method of deposition-precipitation with urea (DPU) method by adopting a literature procedure.[44,55,56] The supported gold catalyst was obtained by using commercial $HAuCl_4.3H_2O$ (Sigma-Aldrich) as a gold precursor and commercial TiO_2 (100% anatase, US research nanomaterials, surface area 50 $m^2\ g^{-1}$, purity = 99.98%) as a support. Briefly, 2 g of TiO_2 was added in a double-wall reactor containing 150 mL of distilled water and an appropriate quantity (27.5 mL) of a solution of gold precursor $HAuCl_4.3H_2O$ to achieve Au loading of 6 wt%. After stirring and heating the solution mixture at 80 °C under stirring, the urea $CO(NH_2)_2$ (Sigma-Aldrich) used as precipitating agent was added in excess to achieve a molar ratio of [urea]/ [metal] = 100. The mixture was stirred at 80 °C in a closed reactor in the dark for 20 h to avoid uncontrolled reduction of gold. The resulting precipitate was separated from the liquid phase by centrifugation and repeatedly washed with distilled water and centrifuged (four times) to remove impurities, in particular residual chlorides. After drying at room temperature overnight, in dark and under vacuum, the catalyst was thermally treated at 300 °C for 2 h under 100 mL min^{-1} of H_2 (Air Liquide, purity 99.999%) at atmospheric pressure, leading to the reduction of the supported gold precursor $HAuCl_4.3H_2O$ into Au metallic nanoparticles. The catalyst was then passivated with N_2 (Air Liquide, purity 99.999%), and finally transferred to air and deposited in a dedicated environmental high-pressure gas cell (HPGC) for *in situ* environmental transmission electron microscopy studies.

In situ environmental transmission electron microscopy

In situ ETEM observations of TiO_2 supported Au NPs under butadiene were performed using a double aberration corrected JEOL ARM 200 F microscope equipped with a cold field emission gun electron source operating at 200 kV. The dedicated environmental high-pressure gas cell (HPGC) used for the *in situ* ETEM observations were provided by Protochips and allowed us to perform atomic level observations of Au nanoparticles at pressures up to atmospheric pressure and temperatures up to 1000 °C. The HPGC consisted of two silicon microelectromechanical system devices called E-chips. These two E-chips have different sizes, with one small non heat conductive and a bigger one heat conductive. The non-conductive E-chip (2 mm × 2 mm × 300 μm) was designed with a 50 nm thick electron-transparent silicon nitride (SiN) window at its center. As for the conductive E-chip (6 mm × 4.5 mm × 300 μm), it was patterned with six windows (2 × 3) 7 μm in diameter holes made up of 30 nm thick electron transparent SiN windows. The two E-chips were precisely aligned and fixed into a closed-cell configuration at the tip of a dedicated TEM sample holder. For *in situ* ETEM observations, the Au catalyst was first grinded then dispersed in distilled water and placed in a sonicator for 15 mins to avoid particle aggregation. The catalyst was then deposited on the large E-chip by drop casting 6 μL of the suspension. All the gases were admitted into the microscope under static gas conditions via a manually-operated gas manifold from Protochips. The sample was heated through resistive heating of the ceramic SiC film on the large E-chip. The dynamic evolution of Au NPs was studied at atmospheric pressure using the following procedure: (i) Initial observation under Ar atmosphere at 300 °C (ii) Exposure to a static mixture of 0.46% C_4H_6/He at 300 °C, and observation during cooling from 300 to 200 °C. *In situ* HAADF and BF-STEM images of Au NPs were recorded using a convergence semi-angle of 20.5 mrad and 17 mrad, respectively. For HAADF imaging, the inner and outer collection semi-angles were equal to 68 and 280 mrad, respectively. To limit the beam irradiation and avoid the damage of NPs, a relatively small probe current of 27 pA with a limited time frame rate of 2 μs per pixel was used, and the electron illumination was blanked between each image acquisition. Atomic-resolution STEM images (2048 × 2048 pixels) were acquired at ×10 M magnification with pixel area equal to 8.97 $\times 10^{-3}$ $Å^2$ corresponding to a dose per frame value equal to 3.7×10^4 $e^-/Å^2$, as defined in reference.[57]

DFT-based MSR model

The morphology changes of Au-NPs of 5 nm size containing 2400 Au atoms under butadiene were quantitatively predicted by a multiscale structure reconstruction (MSR) which combines the Wulff theorem,[58] the Fowler-Guggenheim (F-G) adsorption isotherm[59,60] and DFT calculation of surface energies and interface tensions. All DFT calculated values used for the simulation of the evolution of NP shapes are depicted in Table SI. Definitions of surface energies, interface tensions and average coordination numbers are also provided in the SI.

Supporting Information

Supporting Information is available from the Wiley Online Library or from the author.

Conflict of Interest

The authors declare no conflict of interest.

Acknowledgements

The authors gratefully acknowledge the French National Agency for Research (ANR), grant number ANR-17-CE07-0031" for financial supports.

A.N and J.N would like to thank Dr. Hakim Amara and Dr. Riccardo Gatti for insightful discussions regarding the mechanical properties of metallic nanoparticles and the role of dislocations in their plastic deformation. The authors would also like to thank the five reviewers for their valuable and profound comments.

Keywords: 1,3-butadiene, environmental TEM, gold catalysis, *in situ*, reactivity

References

[1] M. Haruta, N. Yamada, T. Kobayashi, S. Iijima, *Journal of catalysis* **1989**, *115*, 301-309.
[2] P. Claus, *Applied Catalysis A* **2005**, *291*, 222-229.
[3] G.C. Bond, C. Louis, D. Thompson, World Scientific **2006**.
[4] G.C Bond, *Bulletin* **2016**, *49*, 53-61.
[5] B. Qiao, J.X. Liang, A. Wang, J. Liu, T. Zhang, *Chinese Journal of Catalysis* **2016**, *37*, 1580-1586.
[6] S.A, Nikolaev, L.N. Zanaveskin, V.V. Smirnov, V.A. Averyanov, K.L. Zanaveskin, *Russian Chemical Reviews* **2009**, *78*, 231.
[7] L. McEwan, M. Julius, S. Roberts, J.C. Fletcher, *Gold Bull.* **2010**, *43*, 298-306.
[8] M. Wang, Y. Wang, X. Mou, R. Lin, Y. Ding, *Chinese Journal of Catalysis* **2022**, *43*, 1017-1041.
[9] G.C. Bond, P.A. Sermon, G. Webb, D.A. Buchanan, P.B. Wells, *J. Chem. Soc. Chem. Comm.* **1973**, *13*, 444-445.
[10] G.C. Bond, P.A. Sermon, *Bull.* **1973**, *6*, 102–105.
[11] P.A. Sermon, G.C. Bond, P.B. Wells, *J. Chem. Soc. Faraday Trans* **1979**, *75*, 385–394.
[12] M. Okumura, T. Akita, M. Haruta, *Catalysis today* **2002**, *74*, 265-269.
[13] A. Hugon, L. Delannoy, C. Louis, *Gold Bulletin* **2008**, *41*, 127-138.
[14] A. Hugon, L. Delannoy, C. Louis, *Gold Bulletin* **2009**, *42*, 310-320.
[15] I. Horiuti, M. Polanyi, *Transactions of the Faraday Society* **1934**, *30*, 1164-1172.
[16] C. Louis, L. Delannoy, *In Advances in Catalysis*, Academic Press, **2019**, *64*, 1-88.
[17] P.R. Selvakannan, L. Hoang, V.V. Kumar, D. Dumbre, D. Jampaiah, J. Das, S.K. Bhargava, *Catalysis for Clean Energy and Environmental Sustainability* **2021**, 205-228.
[18] S. Chen, B. Yang, *Catalysis Today* **2020**, *347*, 134-141.
[19] S. Naito, M. Tanimoto, *Journal of the Chemical Society, Faraday Transactions 1: Physical Chemistry in Condensed Phases* **1988**, *84*, 4115-4124.
[20] R. Zanella, C. Louis, S. Giorgio, R. Touroude, *Journal of Catalysis* **2004**, *223*, 328-339.
[21] E. Bus, J.T. Miller, J.A. Van Bokhoven, *The Journal of Physical Chemistry B* **2005**, *109*, 14581-14587.
[22] X.F. Yang, A.Q. Wang, Y.L. Wang, T. Zhang, J. Li, *The Journal of Physical Chemistry C* **2010**, *114*, 3131-3139.
[23] R. Meyer, C. Lemire, S.K. Shaikhutdinov, H.J. Freund, *Gold Bulletin* **2004**, *37*, 72-124.
[24] T. Fujitani, I. Nakamura, T. Akita, M. Okumura, M. Haruta, *Angew. Chem. Int. Ed.* **2009**, *48*, 9515–9518.
[25] A. Corma, M. Boronat, S. González, F. Illas, F. *Chemical communications* **2007**, *32*, 3371-3373.
[26] M. Boronat, P. Concepción, A. Corma, *The Journal of Physical Chemistry C* **2009**, *113*, 16772-16784.
[27] K. Ueda, T. Kawasaki, H. Hasegawa, T. Tanji, M. Ichihashi, M. Surface and Interface Analysis: *An International Journal devoted to the development and application of techniques for the analysis of surfaces, interfaces and thin films* **2009**, *40*, 1725-1727.
[28] A. Chmielewski, J. Meng, B. Zhu, Y. Gao, H. Guesmi, H. Prunier, D. Alloyeau, G. Wang, C. Louis, L. Delannoy, P. Afanasiev, *ACS nano* **2019**, *13*, 2024-2033.
[29] M. Arenz, U. Landman, U. Heiz, U. *Chem. Phys. Chem.* **2006**, *7*, 1871-1879.
[30] A. Vargas, G. Santarossa, M. Iannuzzi, A. Baiker, *Physical Review B* **2009**, *80*, 195421.
[31] B. Zandkarimi, P. Poths, A.N. Alexandrova, *Angewandte Chemie* **2021**, *133*, 12080-12089.

[32] D.J. Martin, D. Decarolis, Y.I. Odarchenko, J.J. Herbert, T. Arnold, J. Rawle, C. Nicklin, H.G. Boyen, A.M. Beale, *Chemical Communications* **2017**, *53*, 5159-5162.
[33] Y. Zhu, H. Zhao, Y. He, R. Wang, *Journal of Physics D: Applied Physics* **2021**.
[34] H. Zheng, Y.S. Meng, Y. Zhu, *Mrs Bulletin* **2015**, *40*, 12-18
[35] P.L. Hansen, J.B. Wagner, S. Helveg, J.R. Rostrup-Nielsen, B.S. Clausen, H. Topsøe, *Science* **2002**, *295*, 2053-2055.
[36] F. Ye, M. Xu, S. Dai, P. Tieu, X. Ren, X. Pan, *Catalysts* **2020**, *10*, 779.
[37] H.Zhao, Y. Zhu, H. Ye, Y. He, H. Li, Y. Sun, F. Yang, R. Wang, *Advanced Materials* **2022**, 2206911.
[38] R. Wang, *Nature Catalysis* **2020**, 3, 333-334.
[39] P. Liu, T. Wu, J. Madsen, J. Schiøtz, J.B. Wagner, T.W. Hansen, *Nanoscale* **2019**, 11, 11885-11891.
[40] W. Yuan, B. Zhu, K. Fang, X.Y. Li, T.W. Hansen, Y. Ou, H. Yang, J.B. Wagner, Y. Gao, Y. Wang, Z. Zhang, *Science* **2021**, 371, 517-521.
[41] S. Zhang, P.N. Plessow, J.J. Willis, S. Dai, M. Xu, G.W. Graham, M. Cargnello, F. Abild-Pedersen, X. Pan, *Nano Letters* **2016**, 16, 4528-4534.
[42] X. Du, Y. Huang, X. Pan, B. Han, Y. Su, Q. Jiang, M. Li, H. Tang, G. Li, B. Qiao, *Nature communications* **2020**, 11, 5811.
[43] H. Frey, A. Beck, X. Huang, J.A. van Bokhoven, M.G. Willinger, *Science* **2022**, 376, 982-987.
[44] A. Nassereddine, Q. Wang, D. Loffreda, C. Ricolleau, D. Alloyeau, C. Louis, L. Delannoy, J. Nelayah, H. Guesmi, *Small* **2021**, *17*, 2104571.
[45] Q. Zewei, Y. Wang, J. Fang, *Accounts of Chemical Research* **2013**, *46*, 191-202.
[46] B. Zhu, Z. Xu, C. Wang, Y. Gao, *Nano letters* **2016**, 16, 2628-2632.
[47] M. Duan, J. Yu, J. Meng, B. Zhu, Y. Wang, Y. Gao, *Angewandte Chemie* **2018**, *130*, 6574-6579.
[48] S. De Waele, K. Lejaeghere, M. Sluydts, S. Cottenier, *Physical Review B* **2016**, *94*, 235418.
[49] M.A. Asadabad, M.J. Eskandari, *Electron diffraction, Modern electron microscopy in physical and life sciences* **2016**.
[50] A.F. De Jong, W. Coene, D. Van Dyck, *Ultramicroscopy* **1989**, *27*, 53-65.
[51] D.A. Buchanan, G. Webb, *J. Chem. Soc. Faraday. Trans*. **1975**, *71*,134–144.
[52] Z.R. Ramadhan, A.R. Poerwoprajitno, S. Cheong, R.F. Webster, P.V. Kumar, S. Cychy, L. Gloag, T.M. Benedetti,C.E. Marjo, M. Muhler, D.W. Wang, D.W. *J. Am. Chem. Soc.* **2022**, *144*, 11094–11098.
[53] Z. Li, J.Y. Fu, Y. Feng, C.K. Dong, H. Liu, X.W. Du, *Nat. Catal.* **2019**, *2*, 1107–1114.
[54] Q. Zhu, Z. Pan, Z. Zhao, G. Cao, L. Luo, C. Ni, H. Wei, Z. Zhang, F. Sansoz, J. Wang, *Nat. Commun.* **2021**, *12*, 558.
[55] R. Zanella, S. Giorgio, C.R. Henry, C. Louis,*The Journal of Physical Chemistry B* **2002**, *106*, 7634-7642.
[56] R. Zanella, L. Delannoy, C. Louis, *Applied Catalysis A* **2005**, *291*, 62-72.
[57] P. Abellan, T.J. Woehl, L.R. Parent, N.D. Browning, J.E. Evans, I. Arslan, *Chemical Communications* **2014**, *50*, 4873-4880.
[58] G.X.X.V. Wulff, *Crystalline Materials* **1901**, *34*, 449-530.
[59] I. Langmuir, *Journal of the American Chemical society* **1918**, 40, 1361-1403.
[60] R.H. Fowler, *Statistical thermodynamics* **1939**, CUP Archive.

Table of Contents

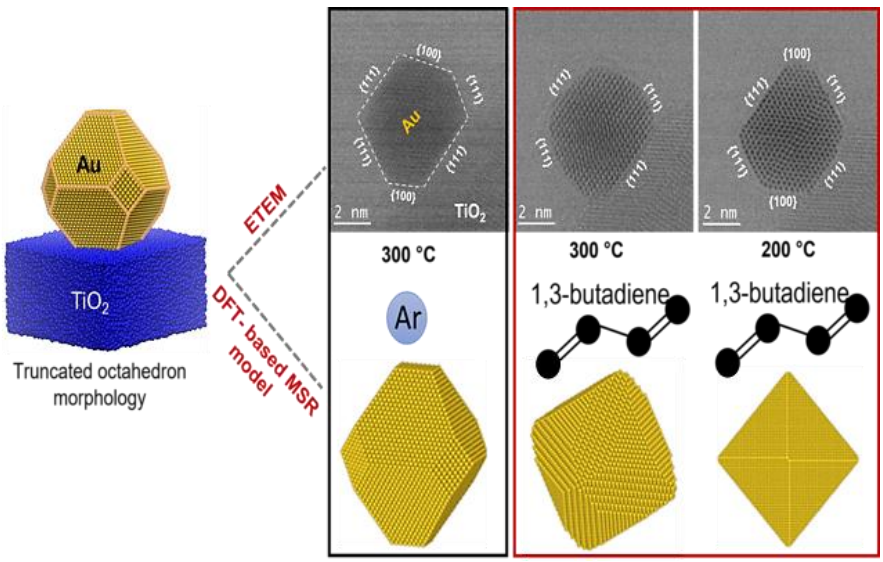

Direct environmental TEM observation of gold nanoparticles under 1,3-butadiene was carried out. Atomic scale *in situ* TEM imaging at single particle level revealed a strong temperature-dependant reactivity of Au NPs towards 1,3-butadiene.